

Article

Snow Patches and Their Influence on Coastal Erosion at Baydaratskaya Bay Coast, Kara Sea, Russian Arctic

Daria Bogatova (Aleksyutina)^{1,*}, Sergey Buldovich² and Vanda Khilimonyuk²

¹ Geoecology of the Northern Territories, Faculty of Geography, Lomonosov Moscow State University, GSP-1, Leninskie Gory, Moscow 119991, Russia

² Geocryology Department, Faculty of Geology, Lomonosov Moscow State University, GSP-1, Leninskie Gory, Moscow 119991, Russia; ser_bul@rambler.ru (S.B.); vanda@geol.msu.ru (V.K.)

* Correspondence: aleksyutina@geogr.msu.ru; Tel.: +7-495-939-2526

Abstract: The Arctic coastal environment is a very dynamic system and sensitive to any changes. In our research we demonstrate that nivation (snow patch activity) impacts the Arctic landscape especially in the coastal dynamic at the western part of Russian Arctic. During fieldwork, snowbanks were described and studied and their qualitative role in the development of coastal systems was revealed for Baydaratskaya Bay coast, the Kara Sea. On one side, the large snow cover protects the coastal slope from thermodenudation and thermoabrasion; on the other side, a thick layer of snow affects the ground temperature regime. During snow melting, snow patches contribute to the removal of material from the coastal slope. The quantitative effect of snow on the ground temperature regime was assessed according to numerical simulations. The critical snow thickness was determined based on a calculation. Critical snow thicknesses based on simulation and field data correlated well. The numerical simulation showed the talik formation under the snow patch. Talik size essentially depends on the freezing temperature of sediment (influenced by salinity). The changes of ground temperature regime might further generate thawing settlement of sediment under snow and contribute to beach topography, which might be a trigger for thermoabrasion.

Keywords: Arctic coast; snow patch; numerical simulation; Kara Sea



Citation: Bogatova (Aleksyutina), D.; Buldovich, S.; Khilimonyuk, V. Snow Patches and Their Influence on Coastal Erosion at Baydaratskaya Bay Coast, Kara Sea, Russian Arctic. *Water* **2021**, *13*, 1432. <https://doi.org/10.3390/w13101432>

Academic Editor: Serafeim E. Poulos

Received: 26 April 2021

Accepted: 17 May 2021

Published: 20 May 2021

Publisher's Note: MDPI stays neutral with regard to jurisdictional claims in published maps and institutional affiliations.



Copyright: © 2021 by the authors. Licensee MDPI, Basel, Switzerland. This article is an open access article distributed under the terms and conditions of the Creative Commons Attribution (CC BY) license (<https://creativecommons.org/licenses/by/4.0/>).

1. Introduction

Climate change in the Arctic region occurs much faster than anywhere else [1,2]. In the previous decades the Arctic seas were covered by sea ice for approximately 9 to 10 months per year [3,4], and the last decade has shown significant decreases in the sea ice extent [5]. Due to climate change, permafrost is warming, too [6]. Snow is one of the main factors affecting the ground temperature regime [7–10]. Snow accumulation increases the ground temperature both in natural conditions [9,11] and during technogenic impact [12]. This can lead to the degradation of permafrost [13], which can be dangerous for Arctic infrastructure and communities [14,15]. The permafrost coasts occupy more than thirty percent of the world's coastline [16]. Erosion rates in the Arctic are the highest in the world [17], and since the 2000s the coastal retreat rate has increased [4,18–20].

The Arctic coasts are complex and actively changing systems. The main coastal destructive processes on the Arctic coasts are thermoabrasion and thermodenudation [19,21–23]. Coastal cliffs of Alaska and the Canadian part of the Beaufort Sea and eastern Russian Arctic, are exposed to active erosion, which entails virtually no beaches on the shore, and the retreat of the edge of the coastal ledges is associated with a “blocky” collapse of frozen rocks in permanent contact with sea water, resulting in niche formation [19,23–28]. The coasts of the western Russian Arctic are composed of permafrost unconsolidated saline sediments [29,30]. Their retreat is associated with thermal degradation of soils during a period with positive air temperatures; the thermodenudation process [31–35]. For different key-sites coasts of the Kara Sea, long-term (30–50 years) average annual retreat rates range

from 0.3 to 2 m/year [36–40]. Another distinctive feature of the Kara sea region is snow patches forming due to snowdrift transport and accumulation, resulting in large amounts of snow in small depressions and on the beach.

The occurrence of snow patches may accelerate coastal erosion. The melting of snow may result in the formation of nival surfaces and niches [41] and promote the removal of eroded material [42]. On the other hand, snow protects the coast from thawing in the early summer [43] and freezing due to extremely cold air temperature during the winter [44].

The aim of this study was to assess the impact of snow patches on coastal erosion and temperature regime. We selected a key site on the southern coast of the Kara Sea, where snow patches of several meters in thickness appear. Their effect was assessed qualitatively, based on field observations, and quantitatively, based on numerical simulations.

2. Study Area

Our research was carried out at the southern Kara Sea coast (Figure 1). The study on this area started in 1988 as a part of engineering site investigations for the construction of the Bovanenkovo-Uhta pipeline for gas transportation from the Yamal Peninsula to Europe. As a key plot, a 5 km long coastal segment between Levdiyev and Torasavey islands was chosen.

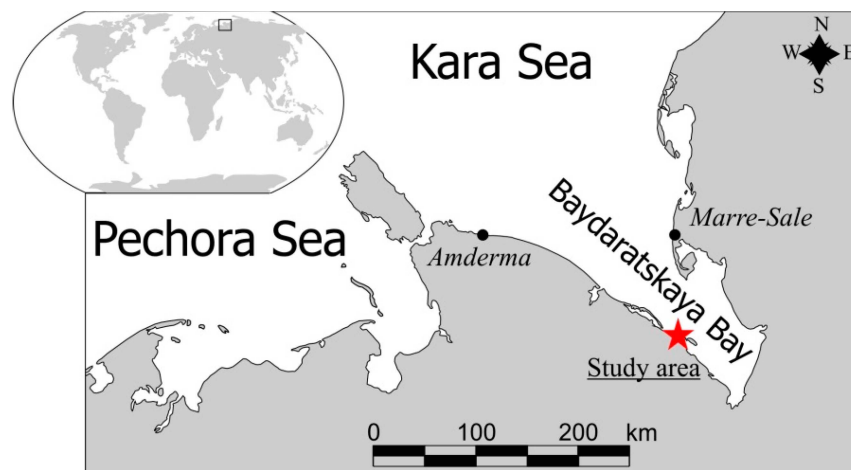


Figure 1. Study area location. The key site is displayed by a star; meteorological stations are shown by circles.

This area is situated in the continuous permafrost zone. Annual ground temperature varies from $-2.4\text{ }^{\circ}\text{C}$ to $-7.5\text{ }^{\circ}\text{C}$. The permafrost thickness on the coasts is more than 50–100 m [3,45]. The coastal cliffs are composed of Late Pleistocene-Holocene [46] frozen unlitified deposits. The lithological composition of cliff sediments varies from loamy clays to sands, and sandy silts prevail [30]. Saline soils are widely present in the geological sections [47] but not everywhere. Since the cliffs are composed of saline soils, freezing temperature of sediments is much lower than $0\text{ }^{\circ}\text{C}$ [48]. As a result, cooled unfrozen sediments interchange with the frozen ones in the permafrost section. In addition, cryopegs also occur. There are several geomorphological levels on the study area: terraces (coastal plain), laida (flood plain) and beach. A 15 to 60 m-wide beach is found along the studied coast. The height of the coastal plain varies from 4 to 6 m (low level) in the eastern part of the studied coastline and up to 12–17 m (high level) in the western part, separated by laida at 1–2.5 m (Figure 2).

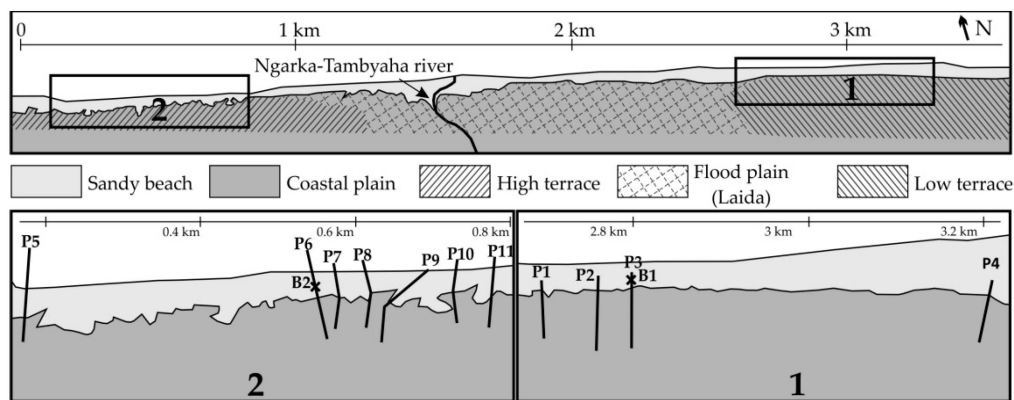


Figure 2. Schema of the 4-km-long coastal segments studied based on different geomorphological levels. Snow patches were surveyed based on geodetic profiles (P) and borehole locations (B).

The territory is characterized by inclement climate. The Kara Sea is covered by sea ice for approximately 9–10 months per year. Annual precipitation is 300–500 mm. In winter, the prevailing wind direction is seaward (from the south); in summer it is inland (from the northwest). During the cold period of the year (air temperature below 0 °C) the prevailing wind velocity is 4–8 m/s (frequency 52%); during the warm period it is 3–6 m/s (50%) [3]. Sometimes, the wind speed can reach 34 m/s [49], which provokes significant snowdrift transport and accumulation of large amounts of wind-blown snow on the beach near the bottom of the coastal slope.

3. Materials and Methods

3.1. Field Work

During fieldwork in June 2012, June and September 2013 and June 2014, the selected coast was observed and snowbanks were discovered. The snow patch size was investigated by a geodetic method using differential GPS (DGPS). A geodetic survey was conducted along the profiles perpendicular to the coastline. We used satellite GNSS receivers from Trimble Inc. (Trimble R8 GPS Receiver, Trimble tsc2 Controller, Trimble HPB450) (Sunnyvale, CA, USA). A reference (base) station was installed, navigational data were collected and corrections using known coordinates were performed. Together with the reference station, the Trimble HPB450 (Sunnyvale, CA, USA) modem transmission equipment was installed, which broadcasted corrections in the CMR + format to a mobile satellite receiver whose internal modem received the correction data. Using DGPS positioning in our conditions allowed an accuracy of about 0.2 m both horizontally and vertically. The survey was performed in real time kinematic (RTK) mode and was carried out in the WGS 84 UTM42N coordinate system. Profile studies were conducted by tachymeter Leica TCR802 power (Canton St. Gallen, Switzerland). Measurements were done on the benchmark and on the distinctive relief points (coastal cliff position, position of coastline, and beach berm), where repeated measurements were made in 10–15 cm increments for better accuracy.

Additionally, in the middle of June 2013, two snow patches were drilled by auger drilling. Borehole 1 was on the beach of the low terrace, and borehole 2 was near the high terrace (Figure 2). The depth of the borehole 1 from the surface of the snow patch was 3 m, and the drilled soil thickness was 1.4 m. Borehole 2 was 4 m deep and did not penetrate the full body of the snow patch. Both boreholes were tubed with plastic pipes. In these boreholes we conducted temperature measurement using thermistor strings M-Log5W (GeoPrecision GmbH) (Ettlingen, Germany).

3.2. Estimation the Critical Thickness of the Snow by Approximate Analytical Methods

An approach to estimate the conditions for the talik was based on the potential depth of thawing ξ_{th} and the potential depth of freezing ξ_f , assuming the temperature is zero

and in the absence of heat fluxes. If the potential depths of seasonally thawing layer and the depths of seasonally freezing layer are equal, the sediments stay in a transitional state [10,50].

In this research, the potential depth of seasonally thawed layer was calculated as [50]:

$$\zeta_{th} = \sqrt{\frac{2 \cdot K_{th} \cdot \Omega_s^c}{L_0} + (K_{th} \cdot R_s^c)^2} - (K_{th} \cdot R_s^c) \quad (1)$$

where K_{th} is the thermal conductivity for sediment in thawed state ($W/(m \cdot K)$), L_0 is the latent heat of fusion (J/m^3), Ω_s^c is the sum of positive air temperature ($^{\circ}C \cdot h$) and R_s^c is the thermal resistance of the cover in summer period ($(m^2 \cdot K)/W$).

The potential depth of seasonally freezing layer was calculated as [50]:

$$\zeta_f = \sqrt{\frac{2 \cdot K_{th} \cdot |\Omega_w^c|}{L_0} + (K_f \cdot (\overline{R_{sn}} + R_s^c))^2} - (K_f \cdot (\overline{R_{sn}} + R_s^c)) \quad (2)$$

where K_{th} is the thermal conductivity for sediment in frozen state ($W/(m \cdot K)$), L_0 is the latent heat of fusion (J/m^3), Ω_w^c is the sum of negative air temperature ($^{\circ}C \cdot h$) and R_{sn} is the thermal resistance of the snow ($(m^2 \cdot K)/W$).

The critical values of the heat transfer parameters that lead to the sediment transition from frozen to thawed state are found from the condition of equality:

$$\zeta_{th} = \zeta_f \quad (3)$$

According to (1), (2) and (3) the critical thermal resistance of the snow layer R_{sn}^{cr} can be calculated as [50]:

$$\overline{R_{sn}^{cr}} = \frac{|\Omega_w^c|}{\zeta_{th} \cdot L_0} - \frac{\zeta_{th}}{2 \cdot K_f} - R_w^c \quad (4)$$

where R_w^c is the thermal resistance of the cover in winter period ($W/(m \cdot K)$).

Knowing the critical thermal resistance and density of the snow cover, the critical height of the snow can be found. For this, the snow thermal conductivity is calculated according to [51]:

$$K_{sn} = 0.021 + 1.01 \cdot 10^{-3} \times \rho_{sn} \quad (5)$$

where ρ_{sn} is the snow density (kg/m^3).

Then the average winter critical snow thickness is:

$$\overline{h_{sn}^{cr}} = \overline{R_{sn}^{cr}} \cdot K_{sn} \quad (6)$$

and for permafrost degradation the maximum critical snow height is approximately [50]:

$$h_{sn}^{cr} \max \approx \overline{h_{sn}^{cr}} \cdot 1.5 \quad (7)$$

A typical average snow density for this region is $\rho_{sn} = 300-400 \text{ kg/m}^3$ [3]. According to the weather station data [52], the sum of positive air temperature was $\Omega_s^c = 17,200 \text{ }^{\circ}C \cdot h$ and the sum of negative air temperature was $\Omega_w^c = -78,300 \text{ }^{\circ}C \cdot h$.

The critical thickness of the snow was estimated for a one-dimension section, where the average annual ground temperature under the snow exceeds the temperature of a freezing point.

3.3. Numerical Simulation

In this study, the simulations were performed using QFrost software (finite-element model) [53], based on the heat balance method for a solution of the enthalpy formulation

of the Stefan problem [54]. Unfrozen water in frozen soils affects the phase transitions [55], which is taken into account according to the formula below:

$$H = \begin{cases} C_f \cdot (T - T_{bf}) + L_0 \rho_d (W_w(T) - W_{tot}) & T < T_{bf}, \\ 0 & T = T_{bf}, \\ C_{th} \cdot (T - T_{bf}) & T > T_{bf}, \end{cases} \quad a = 1, \quad (8)$$

where H is enthalpy (J), L_0 is the latent heat of fusion (J/m^3), T is the temperature ($^{\circ}\text{C}$), T_{bf} is the temperature of freezing point ($^{\circ}\text{C}$), C_f and C_{th} are the heat capacities for frozen and thawed sediments ($\text{J}/(\text{m}^3 \cdot \text{K})$); ρ_d is the bulk density (kg/m^3), W_w is the unfrozen water content (%) and W_{tot} is the total water content (%).

The phase transitions are taken into account as they occur in the range of negative temperatures (depending on unfrozen water content) instead of at fixed temperature.

The upper boundary conditions correspond to the heat exchange processes between air temperatures and frozen soils calibrated with the heat transfer coefficient of the snow. The numerical model assumes that the terrace cliff slopes 45° horizontally. Dimensions of the computational area are 76 m horizontally and 50 m vertically (Figure 3). As the most significant heat exchange processes occur in the seasonal thawing (freezing) layer within the upper 2 m of the soil profile, the upper mesh was set to correspond to elements of 0.1 m, while at greater depths, the block was enlarged to 0.4 m and then to 0.8 m.

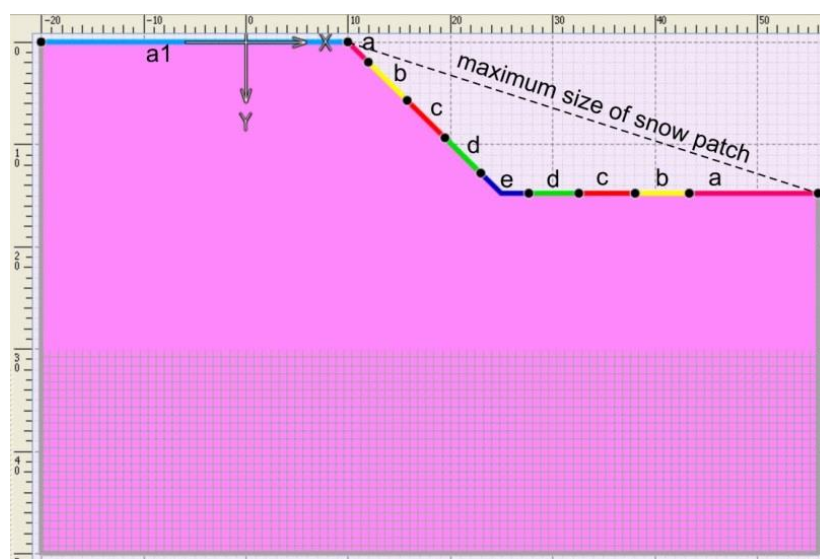


Figure 3. Configuration of a computational space.

There are no field data on the accumulation dynamics of the studied snow patch for the winter period. The model assumes the following change of configuration over time. Intensive snow accumulation due to wind-driven snow mass movements starts at the bottom of the coastal slope. During snow accumulation, the width of the abnormal snow accumulation zone extends up the slope and towards the sea across the beach. At the same time, it is assumed that the growth of the snow patch up to its maximum pre-Spring dimensions occurs as a continuous and consistent process during the entire cold season. At the end of the winter season, the model assumes that the smooth inclined surface of the snow patch starts at the cliff and ends at the beach surface at a distance that is approximately equal to the terrace slope length.

The continuous increase in the thickness and area of the snow is modelled as a series of step-by-step enlargements (four steps of two-month duration). The snow patch size also increases in a step-by-step manner according to the build-up of the snow thickness. The inclined surface of the slope and horizontal surface of the beach are divided into several

zones (a, b, c, d and e in Figure 3). The zones on the terrace slope and on the beach share similar characteristics and widths. In addition, there is a zone characterized by background snow accumulation (a1 Figure 3).

The model assumes an average winter snow thermal conductivity $K_{sn} = 0.35 \text{ W}/(\text{m}\cdot\text{K})$ [3]. Then, for each selected zone, the model calculates the average thickness of the snow cover for a certain time interval between the cycles of step-by-step snow build-up. The heat transfer coefficient ($\alpha_{sn} = 1/R_{sn}$) of the snow layer is calculated as:

$$\alpha_{sn} = K_{sn}/h_{sn}, \quad (9)$$

where K_{sn} is the thermal conductivity of snow ($\text{W}/(\text{m}\cdot\text{K})$) and h_{sn} is the thickness of the snow (m).

Based on the resulting thickness and the thermal conductivity of the snow layer, the model determines the heat transfer coefficient of the snow layer at various time periods for all winter months within the selected zones (Table 1). Long-term average monthly ambient temperatures are based on records drawn from the Mare-Sale weather station located 80 km NE of the study area on the opposite coast of Baydaratskaya Bay [52].

Table 1. Boundary parameters for simulation.

Month	Air Temperature, 0°C	Zone											
		a1		a		b		c		d		e	
		h_{sn}	α_{sn}										
January	−19.8	0.3	1.16	0.3	1.16	0.3	1.16	0.5	0.7	1	0.35	3	0.12
February	−22.6	0.3	1.16	0.3	1.16	0.5	0.7	1	0.35	3	0.12	5	0.07
March	−18.1	0.3	1.16	0.3	1.16	0.5	0.7	1	0.35	3	0.12	5	0.07
April	−12.4	0.3	1.16	0.5	0.7	1	0.35	3	0.12	5	0.07	7	0.05
May	−4.5	0.3	1.16	0.5	0.7	1	0.35	3	0.12	5	0.07	7	0.05
June	3.3 (0.0 ¹)	-	∞										
July	7.4	-	∞										
August	8.3	-	∞										
September	4.6	-	∞										
October	−1.8	0.1	3.5	0.1	3.5	0.1	3.5	0.1	3.5	0.1	3.5	1	0.35
November	−11.8	0.2	1.75	0.2	1.75	0.2	1.75	0.2	1.75	0.2	1.75	1	0.35
December	−16.3	0.3	1.16	0.3	1.16	0.3	1.16	0.3	1.16	0.3	1.16	3	0.12

¹ During the snow patch melting period (June) the temperature of the underlying surface is assumed to be 0°C .

The ground temperature under the snow patch during the melting period (start of the warm season) is set based on the following: at the start of the summer season (June), the upper snow bank surface begins to melt. Water generated as a result of this melting saturates the entire body of the snow patch. At the same time, as the main body of the snow bank maintains a negative temperature, water partially freezes on the ice grains of the snow bank body. However, the volume of such ice reserves is assumed to be small, and temperatures of a subnival soil during the snow melting period (all of June) are assumed to be constant at 0°C .

The input parameters of the sediments composing the coastal slope are set according to laboratory estimations [56–58]. Simulations are performed for saline soils and for nonsaline silty sands, as they dominate on the study area. Soil salinity is assumed close to seawater because the beach is flooded by sea water during strong winds and storms. Considering the possibility of some desalinization by rainwater, the ground freezing temperature is assumed to be $T_{bf} = -1.5^\circ\text{C}$ for saline soils. Other soil parameters such as bulk density ρ_d , total water content W_{tot} , thermal properties and latent heat of fusion are shown in Table 2.

Table 2. Properties of sediments used for simulation.

Soils	W_{tot} , %	ρ_d , kg/(m ³)	K_{th} , W/(m·K)	K_f , W/(m·K)	C_{th} , kJ/(m ³ ·K)	C_f , kJ/(m ³ ·K)	L_0 , kJ/(m ³)
Sandy silt	25	1600	1.5	1.6	2800	2150	107,400

4. Results

4.1. Snow Patches and Their Distribution along the Coast

The field observations showed that in the contact zone between the coastal slope bottom and the beach the snow bodies are up to several tens or hundreds meter wide. Air thawing index or sum of positive air temperatures directly influenced the intensity of thawing or melting. Climatic conditions varied significantly in 2012, 2013 and 2014 (Figure 4). An unusually warm 2012 caused the sea to open at the start of June. Positive air temperature increased faster from the 20th of the May and were never below 0 °C after the 27th of May (Figure 4a). The mean air temperature of June was 8.4 °C. Snow cover had melted on the low terrace and was only found along the beach of the high terrace. Only 25% of the surveyed coastline was covered by snow patches.

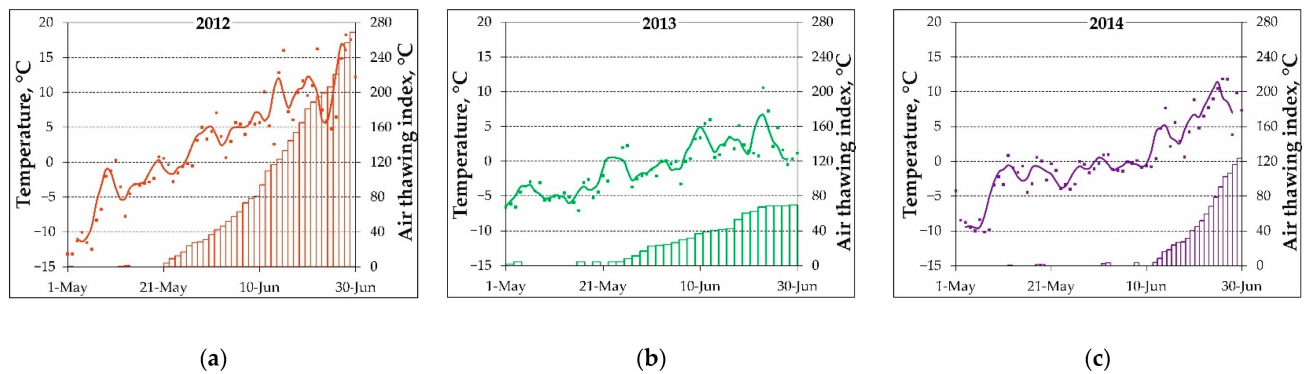


Figure 4. Average daily air temperature and air thawing index (sum of positive air temperatures): (a) May–June 2012; (b) May–June 2013; (c) May–June 2014. Points show the data. Bold lines show the three-days moving average. The bars show the cumulative sum of positive air temperatures (air thawing index).

The next years were colder, preventing the snow from melting early. In 2013, the air temperature and air thawing index slowly increased in May–June (Figure 4b). The mean air temperature was 2 °C in June 2013 and dropped below 0 °C on some days in the middle and end of June. Snow banks covered 58% of the beach along the coastline site and did not occur on laida (flood plain) and on the zones along the high terrace. Snow patch thickness ranged from 1–1.7 m on the beach near the low terrace (profiles 1–4 at Figure 5) and up to 2.7–5.2 m on the beach near high surface (profiles 6–9, 11 at Figure 5). In June 2014, the mean air temperature was 3.8 °C, and positive air temperature increased faster from the 10th of June. In middle of June snow covered 80% of the territory except for a part of laida near the river. At the bottom of the low terrace, the snow thickness varied from 1.6 to 3.5 m (profiles 1–4 at Figure 5). The thickness of the snow layer on the beach at the high terrace ranged from 2.5 up to 6 m (profiles 6–11 at Figure 5). Thus, the snow patch thickness was greater near the high coast than the low terrace, which means the snow thickness depended on the cliff height.

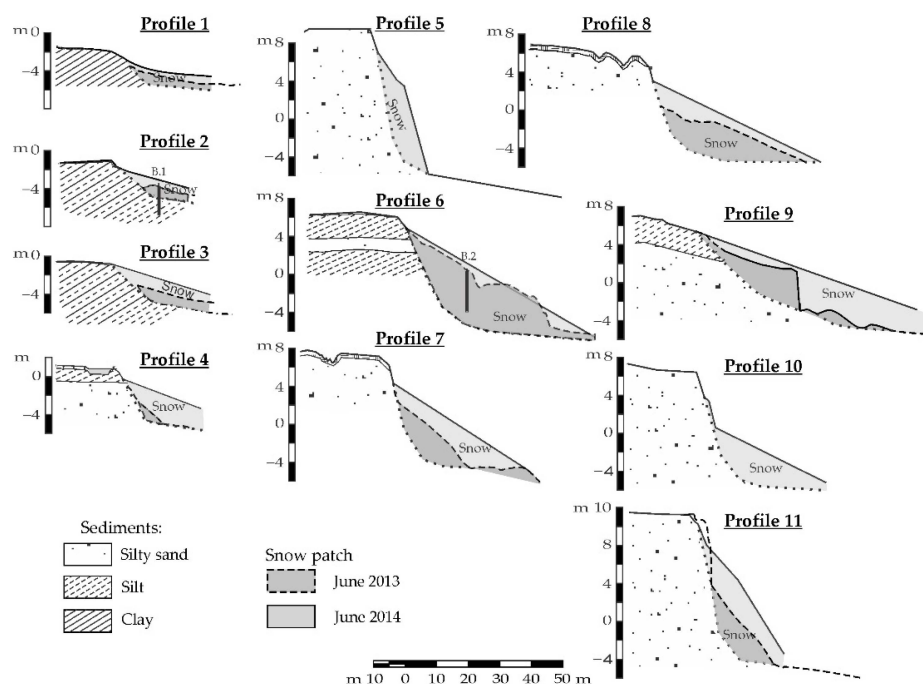


Figure 5. Study area profiles: profiles 1–4—on the low terrace; profiles 5–11—on the high terrace.

The measurements in the borehole 1 showed a temperature in the body of snow of 0 °C (Figure 6). Below the snowpack, sand and silty sediments were drilled. Sand had a low water content near 10%, and water content in the silt was 26–34%. Auger drilling was not able to determine the sediment conditions (thaw or frozen) due to low moisture of the samples and visual absence of ice. The laboratory study assessed the freezing point temperature of deposits as −0.1 to −2.0 °C, but did not accurately reveal the ground state. During field surveys in mid-June 2013, intensive snow melting occurred. The rate of snow surface subsidence near Borehole 1 (relative to the tubing, sealed in the ground) was 0.2–0.3 m/day.

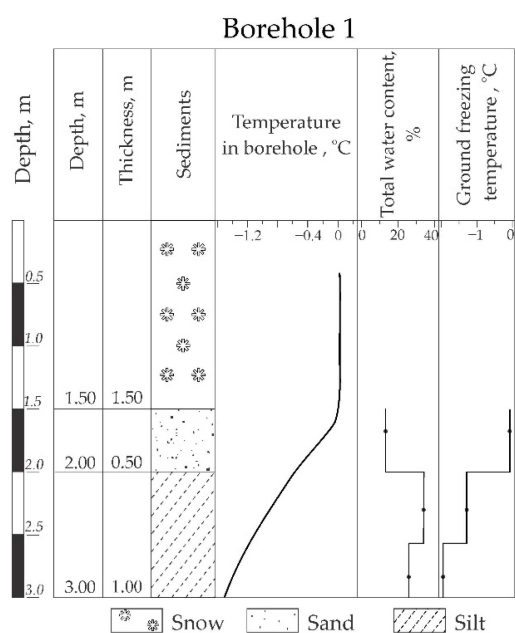


Figure 6. Profile of Borehole 1.

The surface of all the snowbanks remained “dry”, and surface runoff was absent. The two snow patches had different profiles. Near the low surface, in borehole 1, the snow density was approximately constant over the whole profile. Near the high terrace, in borehole 2, we found an ice layer up to 0.5 m at the bottom of the snow patch. Water-saturated zones were formed at the bottom of the snow patch near contact with the beach sediment. The thickness of the water-saturated zone at the base of the snow in the borehole 2 was 0.3–0.4 m.

4.2. Snow Patch Roles in the Coast Dynamic

In June 2012, at the beginning of ice-free period, we observed a niche developing in the snow as a result of repeated wave action. The niches had sizes up to 0.5 m in height and up to several meters in depth (Figure 7).



Figure 7. Wave-cut niches in the coastal snow patch (June 2012).

At the beginning of the warm period, snow patches could mechanically support slope-sliding materials (soil and vegetation cover), thus, decreasing the intensity of thermodenudation in the upper part of the slope above the snow patch (Figure 8). In the lower part of the slope underneath the snowbank, gravity and thaw-induced slope processes were fully blocked when the snow patch was on the beach.



(a)



(b)

Figure 8. Snowbank covered the coast in June 2014: (a) general view of the coast where retreat happened at the upper part of the cliff; (b) thermodenudation created the debris flow at the upper part of the cliff.

During the warm period of the year, during snow melt, we observed water-mud flows from the snow patch towards the sea, as well as water flux inside the snow body (Figure 9). The water flows eroded the coastal slope (Figure 10b), and nival niches were found on the slope of the high terrace (Figure 10a).



Figure 9. Water-mud flows discharging in the body of snow patches: (a) discharge of water-mud flows in the snow patch body; (b) discharge of water-mud flows in the snow patch bottom (June 2013).



Figure 10. Erosion of coastal forms by water flows from collapsing snow patches (June 2012): (a) water flows erode the low part of the coastal slope; (b) nival niche formed by snow patch melting.

4.3. The Estimation of Critical Thickness of Snow

Thermal resistance of the snow for chosen soils properties (Table 2) according to equation (4) was $R = 2.0 - 2.5 \text{ (m}^2 \cdot \text{K)/W}$. Based on Equation (6), the average winter critical thickness of the snow layer for nonsaline soils on the exposed beach surface was only 0.7–0.9 m. Maximum height of the snow layer for the whole winter period corresponding to permafrost degradation was 1.0–1.3 m. One-dimensional modeling, without taking into account changes in the boundary conditions and relief features, showed that if the thermal resistance of the snow increased to around 10–12 $\text{(m}^2 \cdot \text{K)/W}$, the seasonally freezing processes would cease under the snow-bank. This implies that the deposits below the snow patch would stay thawed during the winter period. To reach this value, the average winter snow thickness should be around 3.5–4.2 m, and the maximum snow thickness 5.0–6.0 m. This value of snow patch thickness was observed on the study coast, meaning that, theoretically, talik could form.

4.4. Results of Numerical Simulation Permafrost Conditions under Snow Patch

The results of the numerical simulations for the beginning of snow melting, i.e., for June 1, are given in Figure 11 (for nonsaline soils) and 12 (for saline soils). In both cases, a talik develops under the thick snow bank in the area where the terrace berm meets the beach. The size of the talik mostly depends on the sediments freezing temperature; in saline soils, the talik size is approximately 11 m, which is twice as thick as the talik that develops in nonsaline soils (5 m).

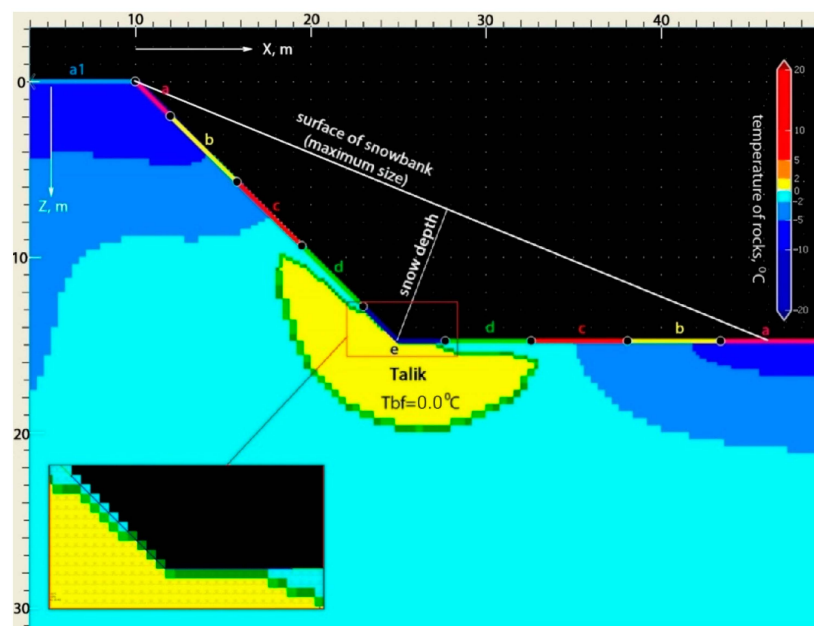


Figure 11. Modelling results for the nonsaline soils. The boundary between the frozen and thawed soils is highlighted in green.

In addition to quantitative specifications, there is also a principal difference in the subsurface sediment conditions related to soil salinity. In case of nonsaline soils, by the end of the cold season (“e” zone), the entire talík is overlaid by an apron of seasonally frozen sediments. Although the thickness of this apron in the “warmest” area next to the edge is small (only 0.1–0.2 m) (see on the inset in bottom left corner Figure 11). In the case of saline soils, sediments in the subsurface zone with a maximum snow patch thickness by the end of the winter season (“e” zone) remain unfrozen (Figure 12). Moreover, starting in early June, seasonally frozen deposits underlying the melting snow patch with a temperature of zero begin to thaw above the remaining talík area, and by the end of June the open part of the talík expands.

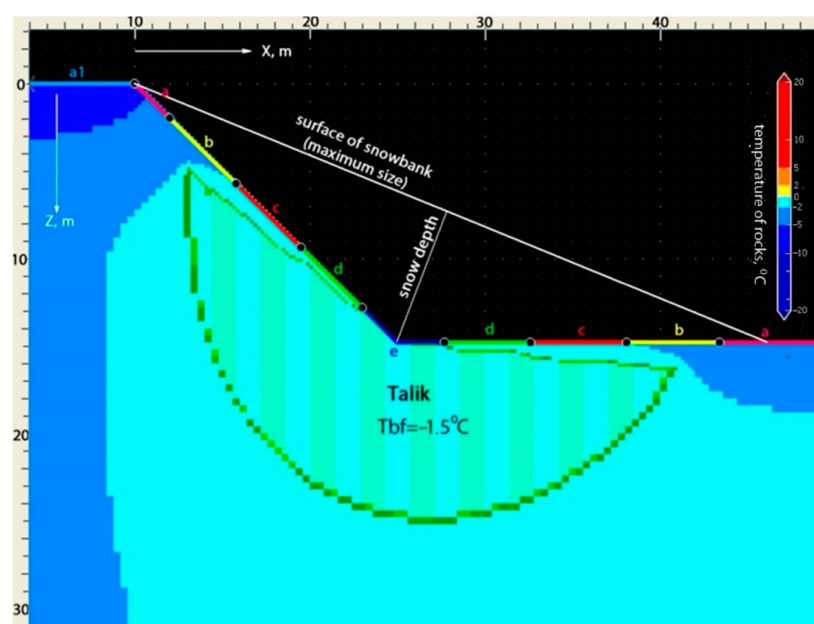


Figure 12. Modelling results for the saline soils. The boundary between frozen and colding soils is highlighted in green.

In addition, according to the simulation data, the seasonally freezing processes would cease under the snow patch and minimum snow thickness should be approximately 5 m for nonsaline soils and only 2 m for saline sediments.

5. Discussion

Our studies showed snow distribution along the coast during different temperatures in May to June. We did not consider the amount of precipitation annually, as is done when studying climate change and its impact on permafrost conditions [8], because at the study areas strong winds occur and snow accumulates in relief depressions. In our case, deflation surfaces completely devoid of vegetation cover were observed on high surfaces, and huge snow patches were found on the beaches, which we attribute to strong winds typical for this area [49]. Snow patches almost are almost absent on the beach near the laida; on these surfaces, and regular snow cover of 0.3 m thickness is present. Such a thickness of snow cover is comparable to the average snow thickness registered at meteorological stations in the study area, which are situated within open flatlands [3]. The temperature of the snow-bank is close to 0 °C at the start of warm season. In winter, the snow patch is cooled well below 0 °C. The cross-section in the snow patch differs depending on different snow thickness, which is associated with cliff height. Near the low terrace at the beginning of the warm period (early spring) melting water penetrates the pore space of the snow cover, partially freezes, partially filtrates below and increases the temperature of the snow patch to 0 °C. If the snow thickness is large, more melting water filters through the snow patch and freezes; this also increases the temperature to 0 °C and results in the formation of an ice layer. The ice layer was directly observed in borehole 2. A temperature of zero of melted water means there is no physical heat for thawing of the initially frozen soil at the bottom of the snow at the very beginning of the warm season. Later, when the daily temperature becomes positive, the melting water filtrates and forms the water-saturated zone. Due to the impermeability of the ice layer, melting water accumulates on top of the ice layer and discharges as water-mud flows from the snow patch to the sea.

The results of our field observations showed that the snow patches have two ambivalent effects on the Baydaratskaya Bay coast. At the beginning of summer, snow protects the coastal slope from solar radiation and air heating (Figure 8) during thermodenudation. Snow patches also protect the coast from direct wave action (thermoabrasion) by preventing waves from reaching the coastal bluff, which is why the niches form in the snow (Figure 7). Similar protective snow patch effects were found at the Yamal-Gydan coastline, Kara Sea [43].

On the other hand, snow patches can enhance coastal destruction. Various large-scale coastal destruction processes have been observed during melting, clearance and sliding of snow, leaving no ambiguities about the destructive capacities of nival processes (Figure 10). During melting periods, these areas generate intensive localized flows that result in thermal erosional degradation of the coastal slope. Thermal erosion and associated mass wasting processes during a 13-day period of snow melting removed approximately 35% of the annual volume of eroded material along the coastline of Yugorskiy Peninsula [42]. At the study coast, the average erosion rates between 2012 and 2015 were estimated as 2–4 m/year for the high surface, 1.2–1.4 m/year for laida and 2.5–4 m/year for the low terrace [59]; therefore, thermodenudation intensity increases and snow melting removes the material from the coastal slope.

Due to global warming, many investigations have noted the thawing settlement of the frozen surface in the Arctic region [60–64]. Thawing settlement in the soil of Arctic coasts varies severely from 1% (in sandy soils) to 55% (in very ice-rich silty soils) [61]. For the Alaska coast [22], 14% of the section lost in 1951–1985 was attributed to thawing settlement. According to laboratory tests [65,66], thawing settlement of samples from the studied area varied from 6 to 31%. As simulations show, the talik sizes depend on the salinity of sediments. For the calculated thickness of the talik in saline soils (11 m), the surface subsidence might be 0.7–3.4 m, and in nonsaline soils (5 m), 0.3–1.55 m. Most likely,

such large surface subsidences are partially compensated by sea activity, when sand washes onto the beach. However, estimated approximations of surface subsidence correspond to those found on the northwest Canada coasts [67], where subsidence during ice melting in soils is more than 3 m. Such large subsidence negatively affects coastal dynamics and causes more active thermoabrasion processes. Moreover, our simulation shows different configurations of talik profiles in saline and nonsaline soils. In the case of nonsaline soils, snow melting water infiltrating the snow body at 0 °C temperature cannot cause thawing of the frozen soils (as melting water offers no additional physical heat) or wash them out (low infiltrating velocity). If the snow patch is positioned on saline sediments, areal washing and soil removal from the snow patch body is theoretically possible during the melting period of the snow patch.

For the study area, the differential snow accumulation leads to different soil temperatures. The average annual ground temperature is -6.2 to -7 °C on the Arctic plain and varies from -2.4 to -4.7 °C in small depressions with an increase in snow accumulation [3]. The presence of such thick snow patches can affect the temperature regime of beach sediments, transferring their state from frozen to thawing. The simulation results showed that under the selected climatic conditions, the critical snow thickness of snow for the talik formation in the seasonally freezing layer was 0.7–1 m, depending on soil salinity, but the critical snow thickness of snow for the seasonally freezing processes would cease under the snow during the winter period at 2–5 m, depending on soil salinity. Such snow thickness could accumulate near low and high cliffs, as our investigation demonstrated. Such cliffs are widespread at the Arctic lowlands and occupy more than 30% of the Kara Sea coast [68].

6. Conclusions

For the study area the snow patches might be continuously distributed for hundreds of meters along the coast or occur as large fragments separated by small sections without snow accumulation. In mid-June, snow patches were present over approximately 30–80% of the surveyed coastline, depending on the climatic conditions of the year. The snow patch thickness depended on the cliff height. At the beginning of the warm season, snow protects the coastal slope from solar radiation, air heating and wave action. Later, snow melting water removes the material from the coastal slope and enhances the thermodenudation processes. Numerical simulation showed that the occurrence of thick snow patches on the beach can produce talik under them. The type and size of taliks depend on salinity of sediments.

Thus, the snow patches on the beach of the study area significantly impact the ground temperature regime and should be taken into account when modelling and forecasting the coastal retreat of the western sector of the Russian Arctic, especially under high coastal slopes, where snow cover of huge thicknesses may occur.

Author Contributions: D.B. field data collection and interpretation, paper writing, review and editing; S.B. field data collection and interpretation, conceptualization, paper writing (first draft methodology of simulation and first draft results), review; V.K. field data collection and interpretation, resources, review. All authors have read and agreed to the published version of the manuscript.

Funding: This article was funded by the Russian Science Foundation, grant number 19-77-00048.

Institutional Review Board Statement: Not applicable.

Informed Consent Statement: Not applicable.

Data Availability Statement: Data is contained within the article.

Acknowledgments: We thank the SAMCoT project for help in fieldwork organization.

Conflicts of Interest: The authors declare no conflict of interest.

References

1. Zakharov, V.F. *Arctic Ice and Modern Natural Processes*; Gidrometeoizdat: Leningrad, Russia, 1981; 136p. (In Russian)
2. Landrum, L.; Holland, M.M. Extremes become routine in an emerging new Arctic. *Nat. Clim. Chang.* **2020**, *10*, 1108–1115. [[CrossRef](#)]
3. Baydaratskaya Bay Environmental Conditions. *The Basic Results of Studies for the Pipeline “Yamal-Center” Underwater Crossing Design*; Publishing House “GEOS”: Moscow, Russia, 1997; p. 432; ISBN 5-89118-008-1. (In Russian)
4. Jones, B.M.; Arp, C.D.; Jorgenson, M.T.; Hinkel, K.M.; Schmutz, J.A.; Flint, P.L. Increase in the rate and uniformity of coastline erosion in Arctic Alaska. *Geophys. Res. Lett.* **2009**, *36*. [[CrossRef](#)]
5. National Snow and Ice Data Center. Available online: <https://nsidc.org/> (accessed on 12 October 2020).
6. Biskaborn, B.K.; Smith, S.L.; Noetzli, J.; Matthes, H.; Vieira, G.; Streletskiy, D.A.; Schoeneich, P.; Romanovsky, V.E.; Lewkowicz, A.G.; Abramov, A.; et al. Permafrost is warming at a global scale. *Nat. Commun.* **2019**, *10*, 264. [[CrossRef](#)]
7. Kudryavtsev, V.A. *Fundamentals of Frost Forecasting in Geological Engineering Investigation*; Nauka Publisher: Moscow, Russia, 1974; p. 431. (In Russian)
8. Stieglitz, M.; Déry, S.J.; Romanovsky, V.E.; Osterkamp, T.E. The role of snow cover in the warming of arctic permafrost. *Geophys. Res. Lett.* **2003**, *30*. [[CrossRef](#)]
9. Zhang, T. Influence of the seasonal snow cover on the ground thermal regime: An overview. *Rev. Geophys.* **2005**, *43*. [[CrossRef](#)]
10. *Principles of the Permafrost Forecast for Engineering and Geological Research*; Publishing House “GeoInfo”: Moscow, Russia, 2016; p. 512; ISBN 978-5-9908493-0-3. (In Russian)
11. Mudryk, L.R.; Kushner, P.J.; Derksen, C.; Thackeray, C. Snow cover response to temperature in observational and climate model ensembles. *Geophys. Res. Lett.* **2017**, *44*, 919–926. [[CrossRef](#)]
12. O’Neill, H.B.; Burn, C.R. Talik Formation at a Snow Fence in Continuous Permafrost, Western Arctic Canada. *Permafr. Periglac. Process.* **2016**, *28*, 558–565. [[CrossRef](#)]
13. Jafarov, E.E.; Coon, E.T.; Harp, D.R.; Wilson, C.J.; Painter, S.L.; Atchley, A.L.; Romanovsky, V.E. Modeling the role of preferential snow accumulation in through talik development and hillslope groundwater flow in a transitional permafrost landscape. *Environ. Res. Lett.* **2018**, *13*, 105006. [[CrossRef](#)]
14. Ospennikov, E.N.; Khilimonyuk, V.Z.; Buldovich, S.N. Typification of geocryological environments of the shelf and coastal zone of the Russian Arctic for the purposes of economic development. In *Proceedings of the Eleventh All-Russian Survey Contractor Conference, Moscow, Russia, 9–11 December 2015*; Publishing House “Academic Science” and LLC “Geomarketing”: Moscow, Russia, 2015; p. 128. (In Russian)
15. Hjort, J.; Karjalainen, O.; Aalto, J.; Westermann, S.; Romanovsky, V.E.; Nelson, F.E.; Etzelmüller, B.; Luoto, M. Degrading permafrost puts Arctic infrastructure at risk by mid-century. *Nat. Commun.* **2018**, *9*, 1–9. [[CrossRef](#)] [[PubMed](#)]
16. Lantuit, H.; Overduin, P.P.; Wetterich, S. Recent Progress Regarding Permafrost Coasts. *Permafr. Periglac. Process.* **2013**, *24*, 120–130. [[CrossRef](#)]
17. Jones, B.M.; Kennen, M.; Hinkel, K.M.; Arp, C.D.; Wendy, R. Eisner Modern erosion rates and loss of coastal features and sites, Beaufort Sea coastline, Alaska. *Arctic* **2008**, *61*, 361–372.
18. Brown, J.; Jorgenson, M.T.; Smith, O.P.; Lee, W. Long-term rates of erosion and carbon input, Elson Lagoon, Barrow, Alaska. In *Proceedings of the 8th International Conference on Permafrost, Zürich, Switzerland, 21–25 July 2003*; pp. 101–106.
19. Günther, F.; Overduin, P.P.; Sandakov, A.V.; Grosse, G.; Grigoriev, M.N. Short- and long-term thermo-erosion of ice-rich permafrost coasts in the Laptev Sea region. *Biogeosciences* **2013**, *10*, 4297–4318. [[CrossRef](#)]
20. Ogorodov, S.; Baranskaya, A.; Belova, N.; Kamalov, A.; Kuznetsov, D.; Overduin, P.; Shabanova, N.; Vergun, A. Coastal dynamics of the pechora and kara seas under changing climatic conditions and human disturbances. *Geogr. Environ. Sustain.* **2016**, *9*, 53–73. [[CrossRef](#)]
21. Zhigarev, L.A. *Submarine Permafrost*; Moscow State University Press: Moscow, Russia, 1997; p. 318. (In Russian)
22. Reimnitz, E.; Are, F.E. 2000 Coastal Bluff and Shoreface Comparison over 34 Years Indicates Large Supply of Erosion Products to Arctic Seas. *Polarforschung* **2000**, *68*, 231–356.
23. Are, F.E. *Coastal Erosion of the Arctic Lowlands*; Academic Publishing House “Geo”: Novosibirsk, Russia, 2012; p. 291; ISBN 978-5-904682-70-5. (In Russian)
24. Kobayashi, N.; Aktan, D. Thermoerosion of Frozen Sediment Under Wave Action. *J. Waterw. Port Coast. Ocean Eng.* **1986**, *112*, 140–158. [[CrossRef](#)]
25. Razumov, S.O. Modeling of the coastal erosion of the Arctic seas in changing climatic conditions Kriosf. *Zemli* **2001**, *1*, 53–60. (In Russian)
26. Barnhart, K.R.; Anderson, R.S.; Overeem, I.; Wobus, C.; Clow, G.D.; Urban, F.E. Modeling erosion of ice-rich permafrost bluffs along the Alaskan Beaufort Sea coast. *J. Geophys. Res. Earth Surf.* **2014**, *119*, 1155–1179. [[CrossRef](#)]
27. Ravens, T.M.; Jones, B.M.; Zhang, J.; Arp, C.D.; Schmutz, J.A. Process-Based Coastal Erosion Modeling for Drew Point, North Slope, Alaska. *J. Waterw. Port Coast. Ocean Eng.* **2012**, *138*, 122–130. [[CrossRef](#)]
28. Korte, S.; Gieschen, R.; Stolle, J.; Goseberg, N. Physical Modelling of Arctic Coastlines—Progress and Limitations. *Water* **2020**, *12*, 2254. [[CrossRef](#)]
29. Brouchkov, A.V. Frozen saline soils of the Arctic coast: Their distribution and engineering properties. In *Proceedings of the 8th International Conference on Permafrost, Zürich, Switzerland, 21–25 July 2003*; pp. 95–100.

30. Aleksyutina, D. Properties of frozen and thawed soils, baydaratskaya bay coast, kara sea: Variability and trends. In *Proceedings of the 18th International Multidisciplinary Scientific GeoConference SGEM2018, Water Resources. Forest, Marine and Ocean Ecosystems, Albena, Bulgaria, 2–8 July 2018*; SGEM: Sofia, Bulgaria, 2018; Volume 18, pp. 397–404. [[CrossRef](#)]
31. Sovershaev, V.A. Tasks of coastal study in the permafrost zone for the purpose of rational economic development. In *Proceedings of Second Conference of geokryologists in Russia, Moscow, Russia, 3–5 June 1996*; Moscow University Press: Moscow, Russia, 1996; Volume 3, pp. 494–503. (In Russian)
32. Kizyakov, A.I. The dynamics of thermodenudation processes at the Yugorsky Peninsula coast Kriosf. *Zemli* **2005**, *9*, 63–68. (In Russian)
33. Aleksyutina, D.; Ogorodov, S.; Shilova, O. Simulation of Coastal Dynamics at the Kara Sea. *J. Coast. Res.* **2020**, *95*, 330–335. [[CrossRef](#)]
34. Ogorodov, S.; Aleksyutina, D.; Baranskaya, A.; Shabanova, N.; Shilova, O. Coastal Erosion of the Russian Arctic: An Overview. *J. Coast. Res.* **2020**, *95*, 599–604. [[CrossRef](#)]
35. Baranskaya, A.; Novikova, A.; Shabanova, N.; Belova, N.; Maznev, S.; Ogorodov, S.; Jones, B.M. The Role of Thermal Denudation in Erosion of Ice-Rich Permafrost Coasts in an Enclosed Bay (Gulf of Kruzenstern, Western Yamal, Russia). *Front. Earth Sci.* **2021**, *8*. [[CrossRef](#)]
36. Vasiliev, A.; Kanevskiy, M.; Cherkashov, G.; Vanshtein, B. Coastal dynamics at the Barents and Kara Sea key sites. *Geo-Marine Lett.* **2005**, *25*, 110–120. [[CrossRef](#)]
37. Kizyakov, A.I.; Leibman, M.O.; Perednya, D.D. Destructive relief-forming processes at the coasts of the Arctic plains with tabular ground ice. *Kriosf. Zemli* **2006**, *2*, 79–89. (In Russian)
38. Kritsuk, L.N.; Dubrovin, V.A.; Yastreba, N.V. Some results of integrated study of the Kara coastal dynamics in the Marre-Sale meteorological station area, with the use of GIS technologies. *Kriosf. Zemli* **2014**, *4*, 59–69.
39. Erosion of permafrost coasts of Kara Sea near Kharasavey Cape, Western Yamal. *Криосфера Земли* **2017**, *6*, 85–97. [[CrossRef](#)]
40. Novikova, A.; Belova, N.; Baranskaya, A.; Aleksyutina, D.; Maslakov, A.; Zelenin, E.; Shabanova, N.; Ogorodov, S. Dynamics of Permafrost Coasts of Baydaratskaya Bay (Kara Sea) Based on Multi-Temporal Remote Sensing Data. *Remote Sens.* **2018**, *10*, 1481. [[CrossRef](#)]
41. Lyubimov, B.P. *On the Mechanism of Nival Processes Underground Ice*; Publishing house of Moscow State University: Moscow, Russia, 1967; pp. 158–175. (In Russian)
42. Gubarikov, A.A.; Leibman, M.O.; Melnikov, V.P.; Khomutov, A.V. The contribution of thermal erosion and thermal denudation in coastal retreat of Ugra Peninsula. *Doklady Akademii Nauk* **2008**, *423*, 543–545. (In Russian)
43. Grigoriev, N.F.; Ermakov, O. Features of processes along Yamal-Gydan coast Kara Sea. In *Coastal Processes in Permafrost*, 1st ed.; Publisher Nauka: Novosibirsk, Russia, 1984; pp. 28–31. (In Russian)
44. Guégan, E.B.M.; Christiansen, H.H. Seasonal Arctic Coastal Bluff Dynamics in Adventfjorden, Svalbard. *Permafr. Periglac. Process.* **2016**, *28*, 18–31. [[CrossRef](#)]
45. Isaev, V.; Koshurnikov, A.; Pogorelov, A.; Amangurov, R.; Podchasov, O.; Sergeev, D.; Buldovich, S.; Aleksyutina, D.; Grishakina, E.; Kioka, A. Cliff retreat of permafrost coast in south-west Baydaratskaya Bay, Kara Sea, during 2005–2016. *Permafr. Periglac. Process.* **2019**, *30*, 35–47. [[CrossRef](#)]
46. Romanenko, F.A.; Belova, N.G.; Nikolaev, V.I.; Olyunina, O.S. Sediments of the Yugorsky coast of Baydaratskaya Bay, Kara Sea. In *Proceedings of the Fifth All-Russian Quaternary Conference, Moscow, Russia, 7–9 November 2007*; Publishing House “GEOS”: Moscow, Russia, 2007; pp. 348–351; ISBN 978-5-89118-401-5. (In Russian)
47. Brouchkov, A. Nature and distribution of frozen saline sediments on the Russian Arctic coast. *Permafr. Periglac. Process.* **2002**, *13*, 83–90. [[CrossRef](#)]
48. Aleksyutina, D.M.; Motenko, R.G. The effect of soil salinity and the organic matter content on the thermal properties and unfrozen water content of frozen soils at the west coast of Baydarata Bay. *Mosc. Univ. Geol. Bull.* **2016**, *71*, 275–279. [[CrossRef](#)]
49. Gerasimov, V.A. Geotechnical monitoring of the new Obskaya—Bovanenkovo railway line. In *Proceedings of the Second International Conference, Collected works No. 19, Moscow, Russia, 7 April 2016*; In Arctic Transport & Logistics; International Transport Academy: Moscow, Russia, 2016; pp. 73–81. ISBN 978-5-7876-0224-1. (In Russian)
50. Buldovich, S.N. Forecasting the formation and development of taliks. In *Fundamental Geocryology. Geocryological Forecast and Environmental Problems in the Permafrost*, 1st ed.; Ershov, E.D., Ed.; Moscow State University Press: Moscow, Russia, 2008; Volume 6, pp. 194–214. (In Russian)
51. Proskuryakov, B.V. *Instructions for Preparing Soil for Development in Winter Conditions*; Bureau of Technical Assistance Gorselstroy: Saint Petersburg, Russia, 1956; p. 18. (In Russian)
52. Weather for 243 Countries of the World. Available online: www.rp5.ru (accessed on 10 September 2018).
53. GitHub. Available online: <https://github.com/kriolog/qfrost> (accessed on 15 November 2016).
54. Khrustalev, L.N.; Cherkasova, L.N. A numerical method for solving the problem of freezing-thawing soil. *Izvestiya Sibirskogo otdeleniya RAS USSR* **1966**, *6*, 12–24. (In Russian)
55. Pustovoi, G.P. Numerical solutions. In *Fundamental Geocryology. Engineering Geocryology*, 1st ed.; Ershov, E.D., Ed.; Moscow State University Press: Moscow, Russia, 1999; Volume 5, pp. 41–55. (In Russian)
56. The composition, structure and properties of frozen and thawed deposits on the Baydaratskaya Bay coast, Kara Sea. *Earths Cryosphere* **2017**, *21*, 11–22. [[CrossRef](#)]

57. Ershov, E.D. *The Thermophysical Properties of Sediments*; Moscow State University Press: Moscow, Russia, 1997; p. 204. (In Russian)
58. Vasil'chuk, Y.K.; Krylov, G.V.; Podborny, E.Y. Cryosphere of oil and gas condensate fields of Yamal peninsula. In *Kharasavey Gas Condensate Field*; Publisher Nedra: Saint Petersburg, Russia, 2006; Volume 1, p. 347. (In Russian)
59. Aleksyutina, D. Using multi-temporal aerial and space imagery for coastal dynamics investigations at kara and pechora seas, russian arctic. In *Proceedings of the 18th International Multidisciplinary Scientific GeoConference SGEM2018, Informatics, Geoinformatics and Remote Sensing, Albena, Bulgaria, 2–8 July 2018*; SGEM: Sofia, Bulgaria, 2018; Volume 18, pp. 265–272. [[CrossRef](#)]
60. Jorgenson, M.T.; Shur, Y.L.; Pullman, E.R. Abrupt increase in permafrost degradation in Arctic Alaska. *Geophys. Res. Lett.* **2006**, *33*. [[CrossRef](#)]
61. Pullman, E.R.; Jorgenson, M.T.; Shur, Y. Thaw Settlement in Soils of the Arctic Coastal Plain, Alaska. *Arctic Antarct. Alp. Res.* **2007**, *39*, 468–476. [[CrossRef](#)]
62. Liu, L.; Schaefer, K.; Gusmeroli, A.; Grosse, G.; Jones, B.M.; Zhang, T.; Parsekian, A.D.; Zebker, H.A. Seasonal thaw settlement at drained thermokarst lake basins, Arctic Alaska. *Cryosphere* **2014**, *8*, 815–826. [[CrossRef](#)]
63. Streletskiy, D.A.; Shiklomanov, N.I.; Little, J.D.; Nelson, F.E.; Brown, J.; Nyland, K.E.; Klene, A.E. Thaw Subsidence in Undisturbed Tundra Landscapes, Barrow, Alaska, 1962–2015. *Permafr. Periglac. Process.* **2016**, *28*, 566–572. [[CrossRef](#)]
64. Antonova, S.; Sudhaus, H.; Strozzi, T.; Zwieback, S.; Kääb, A.; Heim, B.; Langer, M.; Bornemann, N.; Boike, J. Thaw Subsidence of a Yedoma Landscape in Northern Siberia, Measured in Situ and Estimated from TerraSAR-X Interferometry. *Remote Sens.* **2018**, *10*, 494. [[CrossRef](#)]
65. Kotov, P.I. Compressive Deformation in Coastal-Marine Frozen Soil While Thawing (European North Russia, Western Siberia). Ph.D. Thesis, Lomonosov Moscow State University, Moscow, Russia, 3 October 2014.
66. Kotov, P.I.; Roman, L.T.; Tsarapov, M.N. Forecast settlement of frozen soils after thawing. *J. Eng. Heilongjiang Univ.* **2014**, *5*, 1–5.
67. Wolfe, S.A.; Dallimore, S.R.; Solomon, S.M. Coastal permafrost investigations along a rapidly eroding shoreline, Tuktoyaktuk, N.W.T. In *Proceedings of the 7th International Conference on Permafrost, Yellowknife, Northwest Territories, Canada, 23–27 June 1998*; pp. 1125–1131.
68. Kizyakov, A.I.; Ermolov, A.A. Morphodynamic segmentation of the Kara Sea coast In Arctic coasts: The path to sustainability. In *Proceedings of the XXVII International Coastal Conference, Murmansk, Russia, 24–29 September 2018*; Murmansk Arctic State University: Murmansk, Russia, 2018; pp. 92–95; ISBN 978-5-4222-0367-3. (In Russian).